2025 IEEE 33rd International Conference on Network Protocols (ICNP) | 979-8-3315-0376-5/25/$31.00 ©2025 IEEE | DOI: 10.1109/ICNP65844.2025.11192378

SlideLoRa: Reliable Channel Activity Monitoring across Massive Logical Channels in LoRa Networks

Jiamin Jiang*, Shiming Yu†, Hao Wang‡, Haiyang Li§, Yuanqing Zheng†, Lu Wang§
*Nankai University, Tianjin, China
†The Hong Kong Polytechnic University, Hong Kong, China
‡Wuhan University, Wuhan, China
§Shenzhen University, Shenzhen, China
1120250462@mail.nankai.edu.cn, shiming.yu@connect.polyu.hk, hao_wang@whu.edu.cn,
lihaiyang2023@email.szu.edu.cn, yuanqing.zheng@polyu.edu.hk, wanglu@szu.edu.cn

***Abstract*—LoRa technology has been extensively implemented in various IoT applications, offering widespread low-power connectivity for millions of nodes across thousands of logical channels. However, current LoRa networks lack an efficient mechanism for monitoring channel activity across these numerous channels, which prevents network operators from effectively detecting physical layer activities and implementing additional functionalities (*e.g.*, channel access control). Existing solutions either involve complex iterations over each logical channel or fail to detect extremely weak packets in low SNR conditions. These limitations affect their scalability and robustness in monitoring the vast number of logical channels available in the LoRa spectrum. To address this issue, this paper introduces SlideLoRa, an innovative packet detection method that enables detection across all logical channels under various channel conditions. SlideLoRa consolidates the complete energy of LoRa symbols using an expanded demodulation window combined with a fine-grained sliding window, effectively reconstructing the distorted frequency-domain information of LoRa packets. To achieve this, SlideLoRa incorporates a series of novel solutions, including peak tracking in low SNR, peak sequence matching, peak extraction, and packet parameter retrieval. Experimental results demonstrate that SlideLoRa enhances packet detection capability by 1.7× compared to the state-of-the-art.**

***Index Terms*—Low-Power Wide-Area Networks, LoRa, Channel Activity Detection, Cross-Channel.**

I. Introduction

In recent years, Low-Power Wide-Area Networks (LPWANs) have become promising technologies for facilitating widespread connectivity among numerous networked sensors. This advancement supports a variety of IoT applications [1]–[38]. LoRa, featuring its broad coverage and energy efficiency, has been a dominating technology of LPWANs. Industry report [39] indicates that the LoRaWAN ecosystem has connected over 350 million LoRa nodes and 6.9 million gateways worldwide. In many agricultural scenarios, a single LoRa gateway typically serves a large number of LoRa devices within its coverage area, such as sensors deployed across farmland.

To adapt to the ever-increasing scale of IoT networks, LoRa offers thousands of available logical channels with diverse and flexible configurations. Specifically, operating in the unlicensed ISM band (*e.g.*, US902-928 MHz), LoRa nodes can dynamically select the central frequency and available bandwidth (*e.g.*, BW 7.8-500 kHz) to create over 200 physically separated channels. Additionally, LoRa nodes configured with spreading factors (*e.g.*, SF 6-12) can transmit simultaneously on the same frequency. With the narrowband physical channels and orthogonal logical channels, LoRa is well-equipped to connect a vast number of IoT nodes over thousands of available logical channels, shedding light on highly concurrent and scalable IoT connectivity.

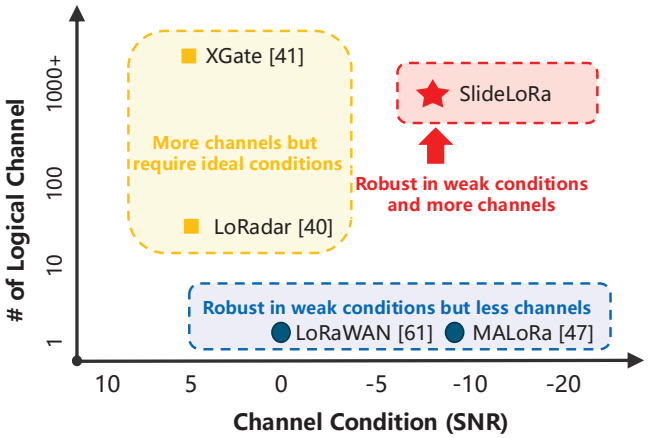

Fig. 1: SlideLoRa achieves high efficiency and reliability to monitor massive logical channels with diverse channel conditions.

The presence of thousands of logical channels presents significant challenges for efficient monitoring of channel activity. Currently, LoRa uses channel activity detection (CAD) to identify activity on a dedicated logical channel, relying on pre-configured channel information (e.g., bandwidth and spreading factor). However, scaling CAD to handle thousands of logical channels would require numerous iterations and introduce substantial overhead, severely impacting network operation efficiency. Although previous research has investigated methods such as cross-channel detection [40] and wideband monitoring [41] to enable concurrent channel activity monitoring, these studies overlook critical issues such as *low-*

979-8-3315-0376-5/25/$31.00 ©2025 IEEE

SNR packets and the near-far effect, which are common in real-world outdoor deployments. Our empirical findings indicate that the reliability of these prior approaches significantly decreases (*e.g.*, $\sim$60%) under conditions of high concurrency and poor channel quality in practical outdoor settings. In this paper, we ask the following question: *Is it possible to efficiently and reliably monitor the channel activity across massive logical channels even under poor channel conditions?*

To answer this question, we first examine why previous approaches lose reliability when handling massive LoRa packets under poor channel conditions. We discover that prior works [40], [41] adhere to the traditional LoRa packet detection approach, which heavily depends on the periodicity of consecutive LoRa symbols for accurate packet detection. This approach performs well when all channels exhibit similarly high signal strengths but fails under poor channel conditions such as low SNR and the near-far effect. One practical issue arises since the symbols of weaker packets (overshadowed by stronger packets) are often overlooked by traditional methods, thus disrupting the periodicity of consecutive LoRa symbols. The problem becomes increasingly challenging when concurrent logical channels with varying signal strengths are also misaligned in time and frequency. Hence, we notice a large gap in existing solutions to supporting reliable channel detection across massive logical channels with diverse channel conditions.

In this paper, we propose SlideLoRa, the first reliable and efficient channel detection system for LoRa networks that monitors all available logical channels with diverse channel conditions. At the core of SlideLoRa is a novel peak feature recovery technique that leverages the impact of window offset on detection results to extract signal features of individual LoRa symbols. By doing so, SlideLoRa can better adapt to diverse channel conditions across massive available logical channels for reliable and efficient detection.

However, implementing this idea into a practical system faces substantial challenges. First, unlike previous works on cross-channel detection, SlideLoRa aims to detect signals from all logical channels in the ISM band under low SNR. This is particularly challenging as poor channel conditions disrupt the periodic characteristics of consecutive LoRa symbols in both time and frequency domains. When packets with different SNR levels are received simultaneously, those with stronger energy dominate in the frequency domain, further distorting the time and frequency domain characteristics of packets with lower SNR levels. Furthermore, the inability to predefine channels to mitigate noise and interference from other channels across the wideband spectrum even worsens SNR degradation. As a result, it is crucially demanding for SlideLoRa to detect and receive packets with high reliability and efficiency.

SlideLoRa introduces novel designs to achieve reliable and efficient channel activity monitoring under diverse channel conditions. We observe that although the carrier frequencies and data rates (SF, BW) of packets from different channels vary, LoRa signals with the same chirp slope (i.e., rate of frequency change over time) can be dechirped simultaneously using a chirp signal with the same chirp slope and the maximum duration (e.g., SF11 and SF12). Built on such observations, SlideLoRa employs only two demodulation windows (chirp signals corresponding to SF11 and SF12) to dechirp and transform energy in the time domain into stable frequency-domain features and detect packets across all channels. Note also that different chirp profiles (e.g., variations in SF and BW) show unique patterns across consecutive demodulation windows. To mitigate the effects of low SNR and near-far interference, SlideLoRa adopts a novel approach by introducing a fine-grained sliding step, which allows SlideLoRa to track the frequency variations of individual chirps across multiple demodulation windows and identify all chirp profiles based on their distinct variation patterns. Subsequently, SlideLoRa detects the periodicity of multiple variation patterns to isolate potential packets in the channels.

We implement and evaluate SlideLoRa with commercial-of-the-shelf (COTS) LoRa nodes and Software Defined Radios (SDR). Evaluations show that SlideLoRa achieves 1.7$\times$ higher packet detection rate than the state-of-the-art (SOTA) in typical outdoor deployments as shown in Figure1.

In summary, the main contributions of this paper are as follows: (1) We propose SlideLoRa, the first system capable of efficiently and reliably monitoring all logical channel activities in a LoRa network under poor channel conditions and without prior knowledge of incoming packets. (2) We introduce a novel packet detection algorithm that fully consolidates the energy of LoRa symbols and leverages multiple periodic features of a single LoRa symbol in the frequency domain, significantly improving detection reliability. (3) We implement extensive experiments and evaluations in real-world outdoor deployments. The experiment results show that SlideLoRa successfully received 82 data packets, even under extremely low SNR channel conditions, achieving a 1.7$\times$ higher packet detection rate compared to baselines.

II. Related Work

Many studies have focused on improving the performance of LoRa networks from various perspectives [42]–[44] , such as spectrum sensing, collision resolution, and packet recovery, which are reviewed as related work in the sequel.

Spectrum Sensing. The goal of spectrum sensing is to detect all potential LoRa packets in the wireless channel [45], [46]. MALoRa [47] enhanced packet detection sensitivity by extending the demodulation window. LoRadar [40] was the first to propose cross-channel packet detection, using the preamble format of LoRa packets to simultaneously identify cross-channel packets within limited bandwidth. XGate [41] further developed novel solutions to detect all LoRa packets in logical channels without any prior knowledge of incoming packets. All these works require relatively good channel conditions, which limits their applicability in real practical scenarios. Unlike the previous work, SlideLoRa aims to reliably detect all logical channels in the Rx spectrum under low SNR conditions.

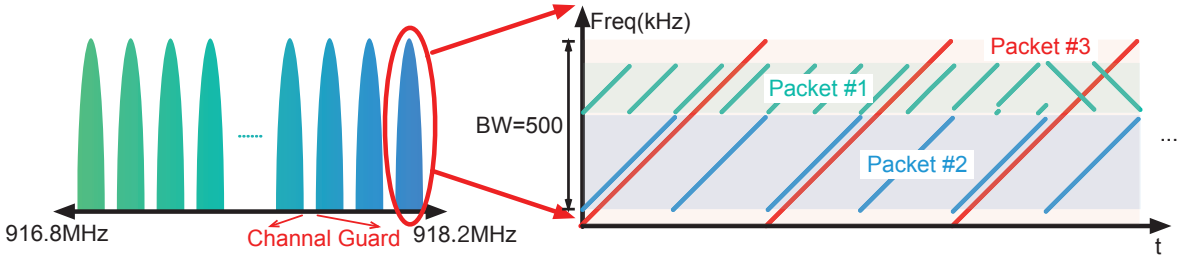

Fig. 2: Physical and Logical Channels in the 915MHz ISM spectrum specified by LoRaWAN. Frequency points are divided into physical channels, while different LoRa parameters define logical channels. Packets #1 (SF7, BW125kHz), #2 (SF9, BW250kHz), and #3 (SF11, BW500kHz) overlap within a 500kHz bandwidth spectrum.

Collision Resolution. Collision resolution in LoRa networks leverages techniques from the physical or MAC layers to fix the issue of packet collisions. At the physical level, Choir exploits hardware imperfections of LoRa nodes to decode colliding packets through unique frequency offsets. FTrack [48], CoLoRa [49], NScale [50], and Pyramid [51] extracted robust features from the time or frequency domain to separate interfering packets. PCube [52] used multiple antennas at the gateway to measure phase differences of colliding packets and group them accordingly. MCLoRa [53] addressed cross-channel packet collisions, which uses energy difference erasers to separate packets from different logical channels. At the MAC layer, LMAC [54] introduced CAD-based CSMA into LoRa networks and significantly reduced packet collisions. However, these studies focus primarily on resolving collisions in a small number of known channels and are never designed to cover all logical channels under poor channel conditions.

Packet Recovery under poor channel conditions. Packet recovery employs various methods such as channel coherent superposition [55], multi-gateway collaboration, and coding features to restore damaged packets [56]. Charm [57] combined signals from multiple LoRaWAN gateways in the cloud to restore weak LoRa signals. OPR [58] analyzed erroneous packets from various gateways in the cloud, trying all possible bit arrangements to restore packet integrity. CPR [59] coherently consolidated FFT results from multiple gateways in the cloud to decode packets below the noise floor. XCopy [60] constructed a combination of signal copies from the same node to achieve ultra-low SNR packet decoding. Despite the performance improvement from these works, they have concentrated only on packet recovery in a single logical channel, without considering SNR loss caused by multiple logical channel superposition.

III. Motivation

This section begins with a brief introduction to the LoRa physical layer. Subsequently, an analysis is presented on the feasibility of despreading multiple distinct logical channels by expanding the demodulation window. Then we discuss the advantages and disadvantages of performing dechirp with an expanded demodulation window to motivate our design.

A. LoRa Background

LoRa Physical Layer. LoRa adopts CSS modulation technology. Specifically, the frequency of a LoRa symbol increases or decreases linearly over time, with the initial frequency of each symbol representing the modulated data. For instance, a symbol encoding the data "00" is a base up-chirp with an initial frequency of zero, with its frequency increasing from $-BW/2$ to $BW/2$. Conversely, a symbol encoding "11" is a data up-chirp with an initial frequency of f_0. When the frequency exceeds $BW/2$, it returns to $-BW/2$ and continues to increase linearly at the same slope.

Physical & Logical Channel. LoRaWAN [61] divides the spectrum (e.g., Sub-1GHz ISM band) into multiple channels. These channels, which do not overlap or interfere with each other, are termed *physical channels*. Currently, commercial LoRa gateways (such as SX1302 [62] or SX1303 [63]) can support simultaneous decoding of up to 8 such physical channels.

In LoRa modulation, chirps can have different changing slopes, defining *logical channels* as shown in Figure 2. That is because when two LoRa chirps with different slopes are transmitted concurrently in the aforementioned physical channel, they will be dispersed into multiple FFT bins after despreading due to their different slopes. This allows the two LoRa chirps to be demodulated without mutual interference.

B. Dechirp-based Concurrent Packet Detection

This section explains how downchirps with identical slopes enable the simultaneous detection of data packets from distinct logical channels. Assuming, without loss of generality, the presence of multiple LoRa packets, let the i-th packet be characterized by a central frequency f_i, bandwidth BW_i, and spreading factor SF_i. Consequently, a base upchirp for each packet can be expressed as:

$$C(SF_i, BW_i, t) = e^{j2\pi\left(-\frac{BW_i}{2}+\frac{k_i}{2}t\right)t}, \quad t \in (0, T_i], \qquad (1)$$

where $k_i = \frac{BW_i^2}{2^{SF_i}}$ is the slope of the linear frequency increase for each base upchirp, and T_i is the symbol duration for that upchirp. A symbol within the packet can then be denoted as:

$$S(f_i, f_0, t) = e^{j2\pi f_0 t} \cdot C(SF_i, BW_i, t), \quad t \in (0, T_i], \qquad (2)$$

where f_0 represents the initial frequency offset encoding the modulated data.

From Eq.(2), it can be observed that if, for example, *the bandwidth doubles while the spreading factor increases by two*, the resulting chirps will possess the same slope k_i despite their differing bandwidths and spreading factors. To better understand the detection process, consider a scenario where the gateway receives two LoRa data packets, packet #1 and packet #2, which share an identical chirp slope $\hat{k}$. Assume packet #2 has twice the symbol duration of packet #1. The received superimposed signal $y(t)$ can be represented as:

$$y(t) = \begin{cases} C(SF_1, BW_1, t_1) & \\ \quad + C(SF_2, BW_2, t_2) & t \in (0, T_1] \\ C(SF_1, BW_1, t_1 + T_1) & \\ \quad + C(SF_2, BW_2, t_2) & t \in (T_1, T_2] \end{cases}, \quad (3)$$

where SF_1, BW_1, T_1 and SF_2, BW_2, T_2 are the spreading factor, bandwidth, and symbol duration for packet #1 and packet #2, respectively. When the gateway employs the base downchirp $conj(C(SF_2, BW_2, t_2))$ to dechirp $y(t)$, followed by a FFT, the result is:

$$\mathcal{F}\{y(t) * conj(C(SF_2, BW_2, t_2))\} = d_1 D_{N_1}(k) + d_1 D_{N_1}(k + \frac{N_1}{2}) + d_2 D_{N_2}(k), \quad (4)$$

where $\mathcal{F}\cdot$ denotes the FFT operation, and N_1 and N_2 are the number of samples per symbol for packet #1 and packet #2, respectively. $D_{N_x}(k)$ represents the Dirichlet kernel, with $D_{N_1}(k) = \frac{\sin(k\pi N_1/N_2)}{\sin(k\pi/N_2)}$ and $D_{N_2}(k) = \frac{\sin(k\pi)}{\sin(k\pi/N_2)}$, having peak heights proportional to N_1 and N_2 respectively. The terms $d_1 = e^{-j(k\pi N_1)/N_2}$ and $d_2 = e^{-jk\pi}$ are phase factors.

Eq. (4) is pivotal because it shows that a base downchirp with a longer symbol duration but the same slope can simultaneously despread base upchirps from multiple packets. In particular, consecutive base upchirps with shorter symbol durations (e.g., those in packet #1) are despread together in a single dechirp operation, producing two distinct peaks for packet #1 in the FFT output. Importantly, the signal strength for each packet is preserved in this process.

C. Why No SNR Loss

As established in Section III-B, specifically by Eq.(4), when two data packets (packet #1 and packet #2) are dechirped using the base downchirp corresponding to packet #2, the FFT output reveals distinct spectral peaks. For packet #1, two such peaks appear, located at frequency bins $k = 0$ (superimposed with a peak from packet #2) and $k = -N_1/2$.

Preservation of Signal Strength. The critical observation from Eq.(4) is that both Dirichlet kernels associated with packet #1 (i.e., $D_{N_1}(k)$ at $k = 0$ and $D_{N_1}(k + N_1/2)$ at $k = -N_1/2$) achieve a peak height proportional to N_1. N_1 represents the total number of samples in a single symbol of packet #1. This signifies that the dechirp operation, even when using the longer demodulation window of packet #2, effectively concentrates the energy of each symbol from packet #1 into a distinct spectral peak of magnitude comparable to that achieved by ideal matched filtering.

To illustrate further, consider the standard dechirping of packet #1 using its own matched base downchirp $conj(C(SF_1, BW_1, t_1))$:

$$\mathcal{F}\{C(SF_1, BW_1, t_1) \cdot conj(C(SF_1, BW_1, t_1))\} \approx d' 1 D N_1(k), \quad (5)$$

where this peak also has a height proportional to N_1. By comparing this ideal scenario with Eq.(4), we see that our proposed method preserves the individual symbol signal strength for packet #1, as evidenced by the peak heights remaining proportional to N_1. Similarly, packet #2's signal energy is concentrated into a peak of height proportional to N_2. Thus, the signal component of the SNR is maintained for each detected symbol.

Noise Considerations. The LoRa waveform inherently possesses a processing gain, which is a key factor in its ability to operate under low SNR conditions. This processing gain arises from the despreading operation (multiplication by the reference chirp followed by FFT).

When the received signal $y(t)$ (which includes additive noise, $n(t)$) is multiplied by the local downchirp $conj(C(SF_2, BW_2, t_2))$, the signal components are coherently integrated (despread) into narrow peaks in the frequency domain, as shown in Eq.(4). Additive White Gaussian Noise (AWGN), on the other hand, is generally uncorrelated with the reference chirp. While the multiplication and FFT operations transform the noise, the despreading process tends to spread the noise energy across the entire frequency band, or at least does not concentrate it in the same way as the signal.

The effective noise power in the narrow frequency bin occupied by the signal peak is therefore significantly lower than the total noise power across the entire bandwidth. The use of a longer dechirp window does not fundamentally alter this property for the shorter symbols of packet #1, as each symbol of packet #1 still correlates over its respective duration T_1 to produce a peak of height N_1. The processing gain for each symbol of packet #1 effectively remains tied to its own parameters (SF_1, BW_1).

Building on the above, we enable the gateway to detect LoRa packets from different channels simultaneously by enlarging the demodulation window for dechirping. By analyzing the FFT output of each demodulation window and applying peak-tracking techniques, we can identify the characteristic peak sequence patterns of each packet for detection. The following section details how these peak sequence patterns are extracted for packets across different channels.

IV. System Design

A. Overview

Traditional LoRa gateways detect packets through correlation of preambles in a known target logical channel. However, correlation detection requires knowing all the meta information

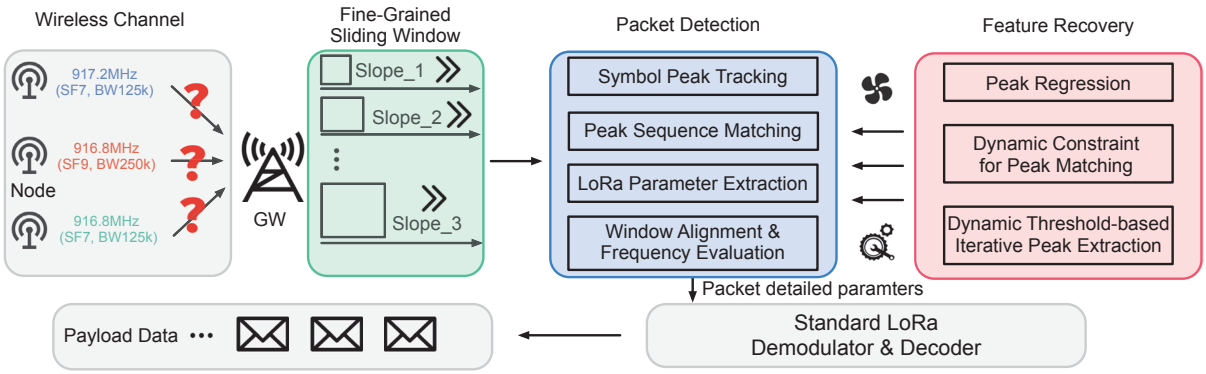

Fig. 3: The workflow of SlideLoRa. SlideLoRa classifies LoRa symbols, detected from different logical channels with unknown channel states using varying slope demodulation windows, for standard LoRa decoding.

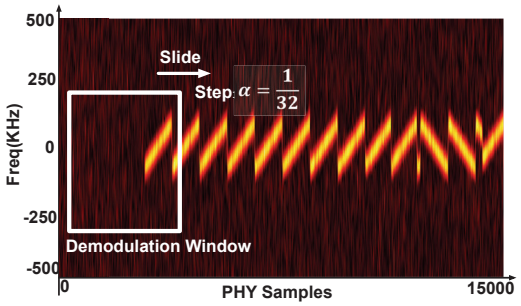

(a) Packet detection process. Packet parameter: (SF7, BW125k), Demodulation Window paramter: (SF12, BW500k).

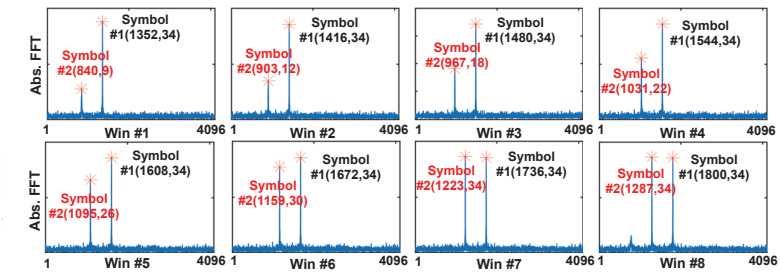

(b) FFT results after dechirp operation in 8 consecutive demodulation windows.

Fig. 4: (a) Packet detection using fine-grained demodulation window shifting. (b) The red peaks originate from the same LoRa symbol and maintain a stable, fixed offset in the FFT results across consecutive windows.

of each packet (e.g., center frequency, SF, and BW) beforehand. This contradicts the original intention of this paper, which aims to enhance the flexibility of channel selection for each node. We observe that, before correlation detection is performed in COTS gateways, the entire received spectrum is low-pass filtered to narrow the signal to the target bandwidth (*e.g.*, BW 62.5-500 kHz). This step aims to eliminate out-of-band noise interference but also limits the gateway's ability to simultaneously detect multiple logical channels. Fortunately, we discover that another packet detection operation can effectively address this problem. Specifically, the dechirp-based packet detection method detects the arrival of packets by observing whether the same FFT bin appears in multiple consecutive demodulation windows. Most importantly, this method can detect packets without filtering the entire spectrum. However, this raises an important question: can the dechirp-based packet detection method be extended to simultaneously detect all potential packets across the entire frequency band?

To answer this question, in this section, we develop novel solutions to concurrently detect multiple packets with different spreading factors and bandwidths in the signal under low SNR without any prior knowledge of incoming packets. As shown in Figure 3, we break down the packet detection process into four steps: 1) Symbol peak tracking: We continuously track the variation patterns of multiple peaks within consecutive windows and extract peaks from the same symbol to form a peak sequence. 2) Peak sequence matching: We identify robust features of the symbols of the same packet in both frequency and time domains and match multiple peak sequences. 3) LoRa parameters extracting: Using the matched peak sequences, we calculate the packet's SF and bandwidth by combining multiple peak sequences. 4) Window aligning and frequency evaluating: To facilitate direct decoding by the decoder, we align multiple packets in both frequency and time domains.

To ensure accurate packet detection in low SNR environments, we thoroughly examine the characteristics of LoRa symbols in the frequency domain and craft three anti-interference algorithms (detailed in section IV-C) tailored to these characteristics to enhance the reliability of our method.

B. Packet Detection over Cross-channel

In this section, we start with a packet and analyze the pattern of peaks from the same symbol in consecutive demodulation windows to construct a peak sequence based on this pattern.

We then match multiple peak sequences to detect packets. Subsequently, we extract the LoRa parameters (SF and bandwidth) of a packet from its multiple peak sequences. Finally, to achieve precise decoding by the decoder, we align the demodulation windows in both frequency and time domains and calculate the carrier frequency offset for each packet.

Symbol Peak Tracking. Through the analysis in Section III-C, we have observed that using a base downchirp with the same slope can simultaneously dechirp multiple base upchirps. When the demodulation window contains all sampling points of a chirp, the SNR loss introduced by the dechirp operation is minimal. Theoretically, we can detect packets by observing whether the same FFT bin exists in consecutive demodulation windows. However, in extremely low SNR scenarios, peak extraction is prone to distortion. This is due to unpredictable shifts in FFT bins with lower energy and the potential misidentification of sidelobes from other high-energy FFT bins as peaks. If peak distortion occurs in any of the consecutive windows, it leads to packet detection failure. In other words, when using the dechirp method for packet detection, it is challenging to detect low-SNR packets using a coarse-grained step size.

To address this issue, as shown in Figure 4, we reduce the step size of the demodulation window to α times $(0 < \alpha < 1)$ its original value:

$$\Delta n = \alpha N, \tag{6}$$

where N is the total sample number of demodulation window. Δn represents the number of sampling points the demodulation window slide. According to the properties of the Fourier transform, FFT bins from the same base upchirp will follow this pattern in the frequency domain due to the movement of the demodulation window as follows:

$$\Delta\text{bin} = \frac{\Delta n \times \Delta f}{\Delta \omega}. \tag{7}$$

Here, $\Delta f = \frac{BW}{N}$ is the frequency shift caused by one sampling point, and $\Delta\omega = \frac{BW}{2^{SF}}$ is the spectral line interval of the FFT result.

We record the index, value, and window number of k-th peak in the FFT results, denoted as $\text{peak}_k = \{\text{index}, \text{value}, \text{number}\}$. Subsequently, based on Eq.(7), we track peaks that differ by Δbin in consecutive demodulation windows and group them into the same peak sequence $PS = \{\text{peak}_1, \text{peak}_2, \cdots \text{peak}_k\}$. We continually create new peak sequences or update existing ones in each FFT round until no peaks remain in the FFT results.

Peak Sequence Matching. After tracking peak sequences, we attempt to match them. We represent peak sequences composed of adjacent base upchirps from a packet as $PS_x = \{\text{peak}_1, \text{peak}_2, \cdots \text{peak}_k\}$ and $PS_{x+1} = \{\text{peak}'_1, \text{peak}'_2, \cdots \text{peak}'_k\}$. Peak sequences originating from the preamble of the same packet exhibit the following characteristics: peaks at the same relative position across all such sequences (e.g., peak_1 in one sequence and peak'_1 in another) tend to have approximately identical index, value, and number attributes, with their value following a consistent variation pattern across sequences, as illustrated in Figure 5. Within any single peak sequence, consecutive peaks (e.g., peak_1 and peak_2) have index values differing by Δbin and number values differing by 1.Based on these characteristics, we match multiple peak sequences. When more than 4 peak sequences are assigned to the same packet, we consider the packet successfully detected.

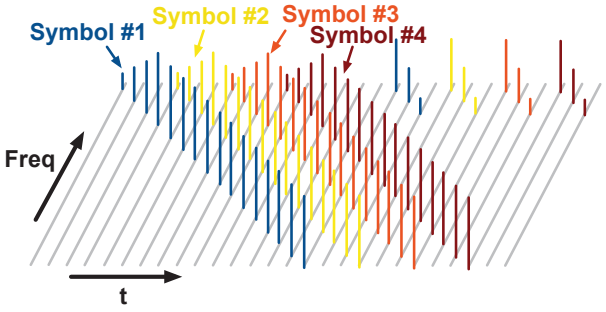

(a) Illustration of peak sequences for different symbols(Symbol #1 $\sim$ #4) from the same packet.

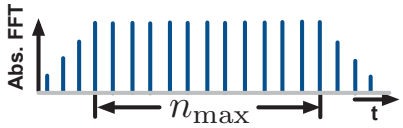

(b) Illustration of $n_{\max}$ peaks.

Fig. 5: Illustration of SlideLoRa extracting the peak sequence of a single LoRa symbol: (a) In consecutive demodulation windows, a single LoRa symbol generates multiple peaks in the frequency domain; (b)$n_{\max}$ peaks are extracted from the unique peak sequence obtained by recording the peaks of Symbol #1 across consecutive demodulation windows.

LoRa Parameter Extracting. After detecting a packet, to facilitate subsequent decoding operations, we need to further analyze the LoRa parameters of this packet, such as SF and BW. Traditional packet detection methods use a base downchirp with the same symbol duration as the target packet as the demodulation window. Once a packet is detected, its SF and BW are identical to those of the base downchirp used.

However, SlideLoRa consistently use a base downchirp with the maximum symbol duration (i.e., SF of 11 or 12) to detect packets. Consequently, we need to adopt a novel approach to extract LoRa parameters. Our method is based on a key insight: symbols with different LoRa parameters have varying durations, resulting in significant differences in the time that the entire symbol remains within the demodulation window during the sliding process as shown in Figure 6.

We quantify this characteristic using the following formula:

$$n_{\max} = \frac{1}{\alpha}\left(\frac{N_w}{N_t} - 1\right) + 1, \tag{8}$$

where $n_{\max}$ represents the number of peaks whose values are approximately equal to the maximum peak value M in the sequence (Figure 5b). Here, *approximately* means that the

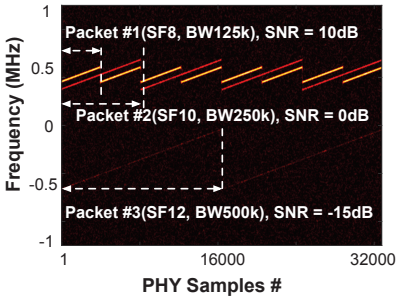

(a) Preambles of 3 packets with different SFs and energy.

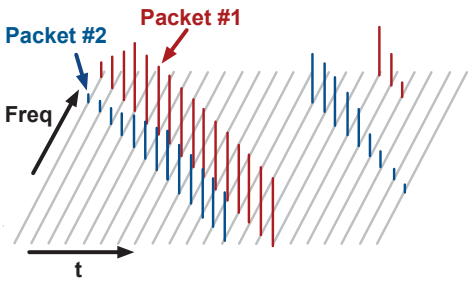

(b) Peak sequences in the frequency domain across consecutive demodulation windows.

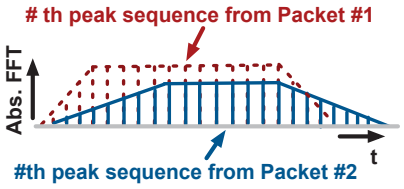

(c) Peak sequences from 2 LoRa symbols with different SFs exhibit significant differences.

Fig. 6: (a) Compound signals of packet #1 in(SF8, BW125kHz), packet #2 (SF10, BW250kHz) and packet #3 in (SF12, BW500kHz); (b-c) Separating collided packets: SlideLoRa leverages distinct peak tracking sequences of different SFs to separate collided packets.

peak value lies within the range $[M(1-\alpha),\ M(1+\alpha)]$, where α is the step-to-window ratio defined in Eq.(6).

From Eq.(8), we can deduce that as the step size of demodulation window decreases, the characteristics distinguishing symbols with different LoRa parameters become more prominent. This enhances our ability to correctly identify different LoRa parameters even under low SNR conditions. However, a smaller step size implies a higher computational overhead. To balance the system's detection performance and overhead, based on our experimental results, we typically set α to 16.

Summary: We extract the LoRa parameters of the packet from the peak sequence through different n_{max}. In LoRa modulation, each symbol is represented by its initial frequency. If the demodulation window is misaligned at the level of sampling points, symbol decoding may fail. The preamble of a LoRa packet serves primarily to enable packet detection and to align the demodulation window before decoding the payload. However, under low-SNR channel conditions, the preamble can be severely degraded by noise, introducing additional challenges. In particular, the received signal may contain multiple overlapping LoRa packets that exhibit the following characteristics:

Window Alignment and Frequency Evaluation. In LoRa modulation, each symbol is represented by its initial frequency. If the demodulation window is misaligned at the level of sampling points, symbol decoding may fail. The preamble of a LoRa packet serves primarily to enable packet detection and to align the demodulation window before decoding the payload. However, under low-SNR channel conditions, the preamble can be severely degraded by noise, introducing additional challenges. In particular, the received signal may contain multiple overlapping LoRa packets that exhibit the following characteristics:

1) *Heterogeneity of Center Frequencies:* Different LoRa nodes may operate on different center frequencies, as they select physical and logical channels based on channel availability and link conditions.
2) *Time Asynchrony:* Packets from different nodes may arrive at the gateway at significantly different times due to independent transmissions and varying wireless propagation paths, resulting in asynchronous arrivals.
3) *Diversity of Carrier Frequency Offsets:* Hardware imperfections in individual LoRa nodes cause each transmitted packet to exhibit a distinct carrier frequency offset.

By discretizing Eq.(2) and setting aside noise considerations, we examine how three primary characteristics determine the structure of the LoRa received signal:

$$S_i(f_i, f_0 + f_{cfo}, n + \Delta n) = e^{j2\pi(f_i+f_0+f_{cfo})(n+\Delta n)} \cdot C(SF_i, BW_i, n+\Delta n), n \in (0, N_i], \tag{9}$$

where N_i is the number of sampling points of the i-th LoRa symbol, and $\Delta n = \lfloor \Delta n \rfloor + \Delta n_\lambda$ is the shift of the demodulation window, consisting of two parts: an integer part $\lfloor \Delta n \rfloor$ and a fractional part Δn_λ. The integer part $\lfloor \Delta n \rfloor$ causes significant frequency shifts, leading to decoding failure, while the fractional part Δn_λ introduces a linear phase shift to the peaks, which has a negligible impact on the decoding result. f_{cfo} is the carrier frequency offset for each packet, and its effect on the demodulation result is similar to that of f_i. We consider f_{cfo} that causes integer bin shifts into f_i for processing and separately estimate the minor f_{cfo}. Similar to previous works [50], [51], we divide the demodulation window alignment and frequency calibration into coarse and fine alignment and calibration steps. Considering that Δn has opposite effects on base upchirps and downchirps in the preamble, while f_i and f_{cfo} have similar effects, we estimate Δn and f_i by combining the peak sequences of base upchirps and downchirps. Note that peaks with lower heights are susceptible to noise or sidelobes, so we use the $n_{\max}$ highest peaks from the peak sequence for estimation.

After obtaining the values of Δn and f_i, we compensate the window for coarse alignment and frequency calibration. Subsequently, we perform another round of dechirp operation

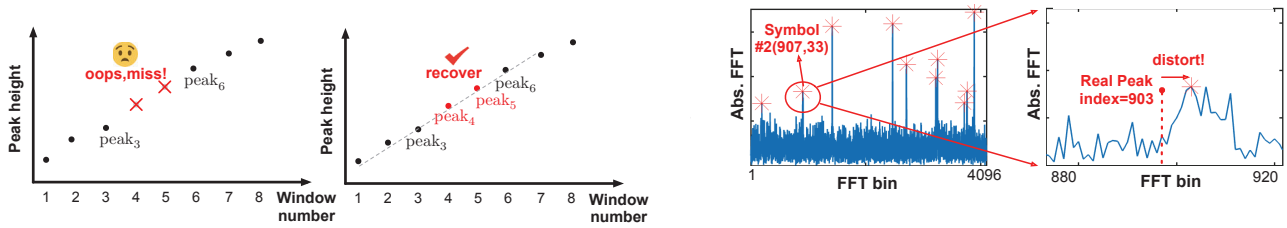

(a) Peak tracking failure in sequences may occur due to interference from multiple concurrent packets.

(b) FFT peaks in the frequency domain may be distorted due to interference from multiple concurrent packets.

Fig. 7: The impact of multiple packets. (a) Peak Regression Algorithm. Approximates missing peaks using existing peak sequence information. (b) Dynamic Constraint for Peak Matching Algorithm. Lower energy peaks are more susceptible to interference, so appropriate matching constraints are selected based on energy levels.

using a demodulation window aligned with the symbol duration of the packet. To improve frequency resolution, zero-padding is applied to the FFT operation to precisely locate the true peak. Finally, we extract the fractional part of the peaks produced by each base upchirp and average them to determine the CFO.

C. Robust Detection on Concurrent packet

In Section IV-B, we provided a detailed explanation of the single packet detection process. This section will discuss how the gateway decodes packets with various slopes when multiple nodes transmit data simultaneously. In conventional LoRa packet transmission, different SF and BW create quasi-orthogonal logical channels. During detection, we treat LoRa packets with different slopes as quasi-orthogonal channels and concurrently detect those with the same slope. In practice, we use 10 different demodulation window sizes with different slope to detect all types of LoRa packets.

However, when the received signal contains LoRa symbols with the same slope and their physical channels significantly overlap, strong inter-packet interference can occur, leading to detection failures. Figure 6 illustrates a scenario where multiple LoRa symbols with the same slope appear within the demodulation window. To improve our method's detection performance under low SNR and packet collision conditions, we propose the following three algorithms.

Peak Regression. As shown in Figure6a, under the near-far effect, LoRa symbols with the same slope but different SFs can easily generate cross-channel interference, causing packet detection to fail for signals with weaker energy. We observe that this is because, during the peak tracking process, some peaks are lost. As shown in Figure7a, we refer back to previous FFT results and compare peak heights and indices across several preceding windows to perform cross-window matching. Finally, we combine multiple FFT results to fit the sequence $\{\text{peak}_i, \ldots, \text{peak}_j\}$, thereby recovering the actual peak sequence. **Dynamic Constraint for Peak Matching.** The process of peak tracking involves determining the difference between the peak indices of the FFT results from two consecutive demodulation windows, referred to as $\Delta\text{bin}'$. When $\Delta\text{bin}'$

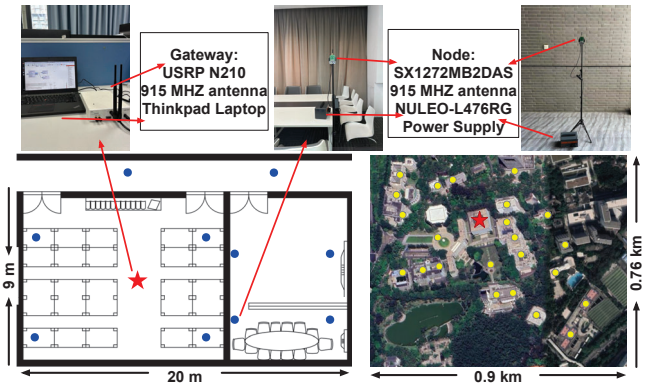

Fig. 8: Testbed settings of SlideLoRa.

satisfies the rule of Eq.(7), that is, $d = \Delta\text{bin}' - \Delta\text{bin} = 0$, we consider these two peaks to belong to the same LoRa symbol. However, under low SNR conditions, peak indices are very fragile and susceptible to noise or other high-energy peaks, causing the peak index to deviate from the ideal value. Therefore, during the peak matching process, we first calculate the energy ratio of this peak $R_{X[k]}$ as shown below.

$$R_{X[k]} = \frac{X[k]}{\sum_{n=1, n\neq k}^{N_F} X[n]}, \tag{10}$$

where N_F is the number of bins in the FFT, and $X[\cdot]$ represents the height of the corresponding peak in the FFT results. If the value of $R_{X[k]}$ is relatively small, we set d to a larger value, thereby allowing a dynamic difference between peak indices and improving the success rate of peak tracking. Note that the setting of d will affect the number of packets detected simultaneously and the accuracy of detection. Therefore, to balance the two, we usually set it in the range of $[1, 20]$ in practice. **Dynamic Threshold-based Iterative Peak Extraction.** To better adapt to varying channel conditions, inspired by previous work [51], we also resort to an iterative peak extraction algorithm along with a dynamic threshold-based peak search method. The basic principle involves first identifying the largest peak in the FFT results and then defining a dynamic threshold $\theta = M + 4\sigma$, where M is the

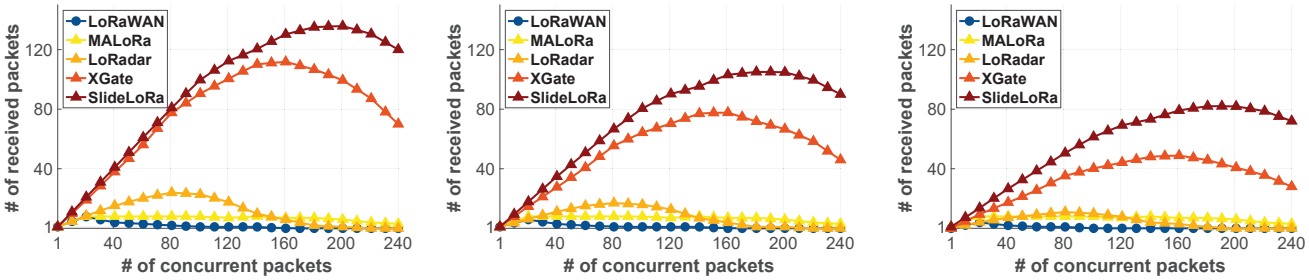

(a) SNR = 10dB (b) SNR = 0dB (c) SNR = -10dB

Fig. 9: The impact of multiple concurrent packets with different SNRs on performance.

mean and σ is the variance of the FFT results. During each iteration of peak extraction, if the maximum value obtained in this round exceeds θ, it is identified as a peak. Subsequently, this maximum value and its surrounding peaks are removed from the FFT results. The threshold θ is then recalculated and updated for the next round of peak extraction. This iterative process continues until the maximum value is less than θ, at which point peak extraction is considered complete.

V. Evaluation

A. Methodology

Gateway. We utilize the USRP N210 software-defined radio platform as a LoRa gateway, implementing its functions through an open-source project [64]. The USRP N210 receives signals from all LoRa nodes at a sampling rate 2MHz, and the physical layer samples are imported into Matlab for offline analysis.

LoRa Nodes. As shown in Figure 8, we deploy LoRa nodes at 20 different locations, each equipped with an SX1272MB2DAS module [65] and an NULEO-L476RG development board. All nodes operate in the 914–916 MHz frequency band, with bandwidths ranging from 62.5 kHz to 500 kHz, and SF chosen arbitrarily from 6 to 12, transmitting across 240 logical channels configured through combinations of 32×62.5 kHz, 16×125 kHz, 8×250 kHz, and 4×500 kHz bandwidths with all spreading factors (SF6–SF12). To enable concurrent transmissions, a dedicated trigger node first broadcasts a trigger packet on a predefined channel; upon reception, all nodes randomly select one of the 240 logical channels to transmit their packets, following the method in [46].

Metrics. We evaluate the performance of SlideLoRa with the following metrics: (1) the number of received packets, which represents the total count of successfully received packets, (2) Packet Detection Rate (PDR), defined as the ratio of correctly detected packets to the total transmitted packets, (3) Symbol Error Rate (SER), which measures the proportion of incorrectly decoded symbols to the total transmitted symbols, and (4) different levels of SNRs, which reflect the quality of the signal environment during packet reception.

Baselines. We compare SlideLoRa with four baselines on channel activity monitoring for LoRa. (1) *LoRaWAN* [61] uses CAD to detect on pre-configured channel; (2) *MALoRa* [47] applies multi-antenna to improve sensitivity; (3) *LoRadar* [40] leverages cross-channel detection to detect multiple logical channels simultaneously; (4) *XGate* [41] detects LoRa packets with diverse configurations across a wide frequency band.

B. Performance of SlideLoRa under different SNRs

We evaluated SlideLoRa against benchmarks across three SNR conditions. LoRaWAN and MALoRa, limited by pre-configured channels and lacking cross-channel detection, received at most 8 packets (Fig. 9). With 200 concurrent packets, SlideLoRa received 136 packets, representing a 17× gain over LoRaWAN/MALoRa. At $\mathrm{SNR} = 10\,\mathrm{dB}$ (Fig. 9a), SlideLoRa detects up to 136 packets, compared with 24 for LoRadar and 112 for XGate, yielding $5.67\times$ and $1.21\times$ improvements, respectively. At $\mathrm{SNR} = 0\,\mathrm{dB}$ (Fig. 9b), the maxima are 104 (SlideLoRa), 10 (LoRadar), and 78 (XGate), i.e., $10.4\times$ and $1.33\times$ gains over the two benchmarks. At $\mathrm{SNR} = -10\,\mathrm{dB}$ (Fig. 9c), packets with $\mathrm{SF} < 8$ become undecodable due to LoRa's modulation limits at such low SNR. In such extreme low-SNR conditions, LoRadar, XGate, and SlideLoRa decode up to 8, 48, and 82 packets, corresponding to $10.25\times$ and $1.7\times$ improvements for SlideLoRa.

C. Performance of SlideLoRa under near-far effect

This experiment assessed PDR under near-far conditions, where gateway-received SNR varies due to node distance and environment. Nodes adjusted SF/BW for successful communication. Received SNRs were grouped: high ($>$ 0 dB; typically SF=7/8), low (-10∼0 dB), and extremely low ($<$ -10 dB; typically SF=11/12). We collected 10-90 concurrent packets per SNR group, totaling 30-270. Figure 10 shows SlideLoRa, XGate, and LoRadar performance. As expected, high-SNR packet PDR gradually decreased with rising concurrency. With 90 concurrent packets per SNR group (270 total), SlideLoRa maintained $>$80% PDR for high-SNR packets (Figure 10a). Lower SNR packets had lower PDR due to high-energy packet interference suppressing their weaker frequency-domain peaks. Yet, with 270 concurrent packets, SlideLoRa achieved 50% PDR for low-SNR and 37% for extremely low-SNR packets, compared to XGate (25% and 15%) and LoRadar (0% and 0%). SlideLoRa's advantage lies in its unique design: beyond

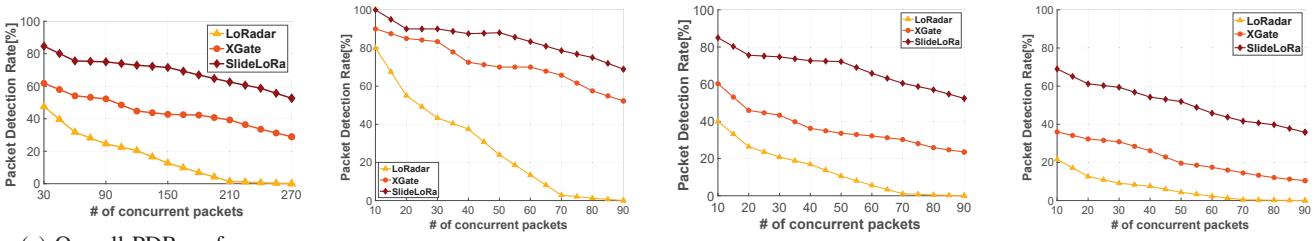

(a) Overall PDR performance (b) High SNR (c) Low SNR (d) Extremely Low SNR

Fig. 10: Near-far effect on packets with different SNR levels. (a) Overall performance of averaged PDR. (b-d) PDRs for packets with high SNR ($>$ 0 dB), low SNR (0 $\sim$ -10 dB), and extremely low SNR ($<$ -10 dB), respectively.

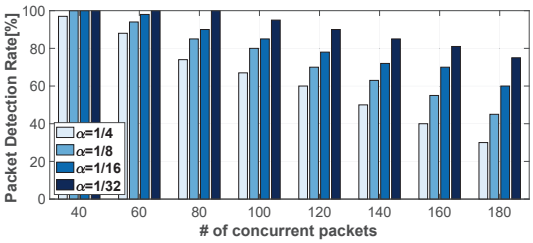

Fig. 11: Performance of SlideLoRa with different ratio of sliding step size

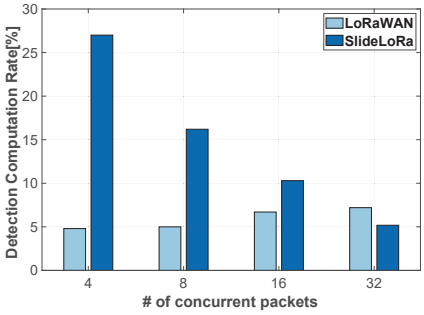

Fig. 12: Preamble computation overhead ratio of SlideLoRa.

preamble periodicity, it uses a fine-grained sliding window to capture distinct peak patterns for varied SF/BW configurations. This enables superior separation of packets with disparate energy levels, significantly improving detection.

D. Microbenchmarks

Impacts of different step sizes of the slide. We evaluate SlideLoRa 's packet detection under different sliding step size ratios α in a high-concurrency scenario (>180 packets). A smaller α means finer sliding granularity. As shown in Fig. 11, reducing α from 1/4 to 1/32 significantly improves detection performance; at $\alpha = 1/32$, detection remains above 80% even with 160 concurrent packets. In contrast, larger steps (e.g., $\alpha = 1/4$) cause performance to drop sharply, as detection degrades to conventional LoRa's periodic upchirp method, reducing sensitivity in complex high-concurrency environments.

Computation Overhead of SlideLoRa. We define the *detection computation ratio* as the computation in the preamble detection stage divided by the number of packets detected in a single detection sweep. We compare this ratio for SlideLoRa ($\alpha = 1/8$) and LoRaWAN over a 2 MHz band with concurrent packets (BW 62.5–500 kHz, SF 7–12). In LoRaWAN, each packet requires its own preamble detection, so the ratio remains almost constant regardless of the number of concurrent packets. In contrast, SlideLoRa performs a single, more computationally intensive preamble detection—about $1/\alpha$ times the cost of LoRaWAN's—that can detect all concurrent packets in the same slope group. When the number of concurrent packets is small, this extra cost is not amortized, resulting in a much higher ratio. As concurrency increases, the detection cost is distributed across more packets, and the per-packet detection computation ratio decreases rapidly. At 32 concurrent packets, SlideLoRa's ratio becomes lower than that of LoRaWAN.

VI. Conclusion

This paper presents SlideLoRa, a reliable and efficient system for monitoring channel activity across massive logical channels in LoRa networks under poor channel conditions. By leveraging a fine-grained sliding demodulation window and innovative peak feature recovery techniques, SlideLoRa effectively detects packets without any prior knowledge of incoming packets' configurations, even in extremely low SNR ($<$ -10 dB) environments. Extensive real-world experiments demonstrate that SlideLoRa achieves a 1.7$\times$ improvement in packet detection compared to benchmark methods, significantly enhancing the scalability and reliability of LoRa networks for large-scale IoT deployments.

Acknowledgment

We sincerely thank the anonymous shepherd and reviewers for their valuable comments and feedback. This work was supported in part by the China NSFC Grant (No. 62372307, No. U2001207), Guangdong NSF (No. 2024A1515011691), Shenzhen Science and Technology Program (No. RCYX20231211090129039), Shenzhen Science and Technology Foundation (No. JCYJ20230808105906014), Guangdong Provincial Key Lab of Integrated Communication, Sensing, and Computation for Ubiquitous Internet of Things (No. 2023B1212010007), the Project of DEGP (No. 2023KCXTD042), and Hong Kong GRF (Grant No. 15206123, 15211924). Lu WANG is the corresponding author.

REFERENCES

[1] W. He, W. Wu, X. Gu, and Z. Chen, "Diff-adf: Differential adjacent-dual-frame radio frequency fingerprinting for lora devices," in *IEEE INFOCOM 2024-IEEE Conference on Computer Communications*. IEEE, 2024, pp. 2089–2098.

[2] Z. Wang, H. Zhu, Y. Cai, Q. Liu, S. Chang, and L. Zhang, "Lorapcr: Long range point cloud registration through multi-hop relays in vanets," in *IEEE INFOCOM 2024-IEEE Conference on Computer Communications*. IEEE, 2024, pp. 1311–1320.

[3] F. Yu, X. Zheng, Y. Ma, L. Liu, and H. Ma, "Resolve cross-channel interference for lora," in *2024 IEEE 44th International Conference on Distributed Computing Systems (ICDCS)*. IEEE, 2024, pp. 1027–1038.

[4] K. Yang, Y. Chen, and W. Du, "Orchloc: In-orchard localization via a single lora gateway and generative diffusion model-based fingerprinting," in *Proceedings of the 22nd Annual International Conference on Mobile Systems, Applications and Services*, 2024, pp. 304–317.

[5] C. Li, Y. Ren, S. Tong, S. I. Siam, M. Zhang, J. Wang, Y. Liu, and Z. Cao, "Chirptransformer: Versatile lora encoding for low-power wide-area iot," in *Proceedings of the 22nd Annual International Conference on Mobile Systems, Applications and Services*, 2024, pp. 479–491.

[6] C. Shao and O. Muta, "Tonari: Reactive detection of close physical contact using unlicensed lpwan signals," *ACM Transactions on Internet of Things*, vol. 5, no. 2, pp. 1–30, 2024.

[7] L. Shen, Q. Yang, K. Cui, Y. Zheng, X.-Y. Wei, J. Liu, and J. Han, "Fedconv: A learning-on-model paradigm for heterogeneous federated clients," in *Proceedings of the 22nd Annual International Conference on Mobile Systems, Applications and Services*, 2024, pp. 398–411.

[8] Y. Ren, W. Sun, J. Du, H. Zeng, Y. Dong, M. Zhang, S. Chen, Y. Liu, T. Li, and Z. Cao, "Demeter: Reliable cross-soil lpwan with low-cost signal polarization alignment," in *Proceedings of the 30th Annual International Conference on Mobile Computing and Networking*, 2024, pp. 230–245.

[9] S. Yu, X. Xia, Z. Zhang, N. Hou, and Y. Zheng, "Fdlora: Tackling downlink-uplink asymmetry with full-duplex lora gateways," in *Proceedings of the 22nd ACM Conference on Embedded Networked Sensor Systems*, 2024, pp. 281–294.

[10] Y. Chen, K. Yang, Z. An, B. Holder, L. Paloutzian, K. M. Bali, and W. Du, "Marlp: Time-series forecasting control for agricultural managed aquifer recharge," in *Proceedings of the 30th ACM SIGKDD Conference on Knowledge Discovery and Data Mining*, 2024, pp. 4862–4872.

[11] B. Hou and J. Wang, "Lobaca: Super-resolution lora backscatter localization for low-cost tags," in *IEEE INFOCOM 2024-IEEE Conference on Computer Communications*. IEEE, 2024, pp. 1081–1090.

[12] J. Lin, R. Xiong, Z. Xu, W. Tian, C. Chen, X. Dong, and J. Luo, "Multi-node concurrent localization in lora networks: Optimizing accuracy and efficiency," in *IEEE INFOCOM 2024-IEEE Conference on Computer Communications*. IEEE, 2024, pp. 1091–1100.

[13] J. Du, Y. Ren, Z. Zhu, C. Li, Z. Cao, Q. Ma, and Y. Liu, "Srlora: Neural-enhanced lora weak signal decoding with multi-gateway super resolution," in *Proceedings of the Twenty-fourth International Symposium on Theory, Algorithmic Foundations, and Protocol Design for Mobile Networks and Mobile Computing*, 2023, pp. 270–279.

[14] A.-U.-H. Ahmar, E. Aras, T. D. Nguyen, S. Michiels, W. Joosen, and D. Hughes, "Design of a robust mac protocol for lora," *ACM Transactions on Internet of Things*, vol. 4, no. 1, pp. 1–25, 2023.

[15] Z. Wang, L. Kong, L. Shangguan, L. He, K. Xu, Y. Cao, H. Yu, Q. Xiang, J. Yu, T. Ma *et al.*, "Ligbee: Symbol-level cross-technology communication from lora to zigbee," in *IEEE INFOCOM 2023-IEEE Conference on Computer Communications*. IEEE, 2023, pp. 1–10.

[16] B. Xie, M. Cui, D. Ganesan, X. Chen, and J. Xiong, "Boosting the long range sensing potential of lora," in *Proceedings of the 21st Annual International Conference on Mobile Systems, Applications and Services*, 2023, pp. 177–190.

[17] S. Tong, J. Wang, J. Yang, Y. Liu, and J. Zhang, "Citywide lora network deployment and operation: Measurements, analysis, and implications," in *Proceedings of the 21st ACM Conference on Embedded Networked Sensor Systems*, 2023, pp. 362–375.

[18] X. Xia, Q. Chen, N. Hou, and Y. Zheng, "Hylink: Towards high throughput lpwans with lora compatible communication," in *Proceedings of the 20th ACM Conference on Embedded Networked Sensor Systems*, ser. SenSys '22. New York, NY, USA: Association for Computing Machinery, 2023, p. 578–591. [Online]. Available: https://doi.org/10.1145/3560905.3568516

[19] N. Hou, X. Xia, Y. Wang, and Y. Zheng, "One shot for all: Quick and accurate data aggregation for lpwans," in *IEEE INFOCOM 2023 - IEEE Conference on Computer Communications*, 2023, pp. 1–10.

[20] Y. Song, L. Lu, J. Wang, C. Zhang, H. Zheng, S. Yang, J. Han, and J. Li, "{μMote}: enabling passive chirp de-spreading and {μW-level}{Long-Range} downlink for backscatter devices," in *20th USENIX symposium on networked systems design and implementation (NSDI 23)*, 2023, pp. 1751–1766.

[21] D. Guo, C. Gu, L. Jiang, W. Luo, and R. Tan, "Illoc: In-hall localization with standard lorawan uplink frames," *Proceedings of the ACM on Interactive, Mobile, Wearable and Ubiquitous Technologies*, vol. 6, no. 1, pp. 1–26, 2022.

[22] X. Guo, L. Shangguan, Y. He, N. Jing, J. Zhang, H. Jiang, and Y. Liu, "Saiyan: Design and implementation of a low-power demodulator for {LoRa} backscatter systems," in *19th USENIX Symposium on Networked Systems Design and Implementation (NSDI 22)*, 2022, pp. 437–451.

[23] Z. Zhao, W. Gao, W. Du, G. Min, W. Mao, and M. Singhal, "Towards energy-fairness in lora networks," *IEEE Transactions on Mobile Computing*, vol. 22, no. 9, pp. 5597–5610, 2022.

[24] X. Tian, J. Sarkis, W. Chen, Y. Geng, H. Pan, Z. Liu, and S. Ulgiati, "Greening the belt and road initiative: Evidence from emergy evaluation of china's provincial trade with asean countries," *Fundamental Research*, 2022.

[25] K. Yang and W. Du, "Lldpc: A low-density parity-check coding scheme for lora networks," in *Proceedings of the 20th ACM Conference on Embedded Networked Sensor Systems*, 2022, pp. 193–206.

[26] S. Tong, Y. He, Y. Liu, and J. Wang, "De-spreading over the air: long-range ctc for diverse receivers with lora," in *Proceedings of the 28th Annual International Conference on Mobile Computing and Networking*, 2022, pp. 42–54.

[27] N. Hou, X. Xia, and Y. Zheng, "Jamming of lora phy and countermeasure," in *IEEE INFOCOM 2021 - IEEE Conference on Computer Communications*, 2021, pp. 1–10.

[28] C. Li, H. Guo, S. Tong, X. Zeng, Z. Cao, M. Zhang, Q. Yan, L. Xiao, J. Wang, and Y. Liu, "Nelora: Towards ultra-low snr lora communication with neural-enhanced demodulation," in *Proceedings of the 19th ACM Conference on Embedded Networked Sensor Systems*, 2021, pp. 56–68.

[29] C. Gu, L. Jiang, R. Tan, M. Li, and J. Huang, "Attack-aware synchronization-free data timestamping in lorawan," *ACM Transactions on Sensor Networks (TOSN)*, vol. 18, no. 1, pp. 1–31, 2021.

[30] Z. Xu, S. Tong, P. Xie, and J. Wang, "Fliplora: Resolving collisions with up-down quasi-orthogonality," in *2020 17th Annual IEEE International Conference on Sensing, Communication, and Networking (SECON)*. IEEE, 2020, pp. 1–9.

[31] X. Guo, L. Shangguan, Y. He, J. Zhang, H. Jiang, A. A. Siddiqi, and Y. Liu, "Aloba: Rethinking on-off keying modulation for ambient lora backscatter," in *Proceedings of the 18th conference on embedded networked sensor systems*, 2020, pp. 192–204.

[32] S. Yu, Z. Zhang, X. Xia, Y. Zheng, and J. Wang, "Are lora logical channels really orthogonal? practically orthogonalizing massive logical channels," in *ACM MobiSys*, 2025.

[33] N. Hou, Y. Wang, X. Xia, S. Yu, Y. Zheng, and T. Gu, "Molora: Intelligent mobile antenna system for enhanced lora reception in urban environments," in *ACM SenSys*, 2025, pp. 424–436.

[34] R. Li, Z. Zhang, X. Xia, N. Hou, W. Chai, S. Yu, Y. Zheng, and T. Gu, "From interference mitigation to toleration: Pathway to practical spatial reuse in lpwans," *ACM MobiCom*, 2025.

[35] Y. Ren, P. Cai, J. Jiang, J. Du, and Z. Cao, "Prism: High-throughput lora backscatter with non-linear chirps," in *IEEE INFOCOM*, 2023, pp. 1–10.

[36] Y. Ren, A. Gamage, L. Liu, M. Li, S. Chen, Y. Dong, and Z. Cao, "Sateriot: High-performance ground-space networking for rural iot," in *ACM MobiCom*, 2024.

[37] N. Hou, X. Xia, and Y. Zheng, "Cloaklora: A covert channel over lora phy," *IEEE/ACM Transactions on Networking*, 2022.

[38] S. Tong, Z. Shen, Y. Liu, and J. Wang, "Combating link dynamics for reliable lora connection in urban settings," in *ACM MobiCom*, 2021, pp. 642–655.

[39] Semtech. (2024, Mar.) Lora. "https://www.semtech.com/lora".

[40] F. Yu, X. Zheng, L. Liu, and H. Ma, "Loradar: An efficient lora channel occupancy acquirer based on cross-channel scanning," in *IEEE INFOCOM 2022-IEEE Conference on Computer Communications*. IEEE, 2022, pp. 540–549.

[41] S. Yu, X. Xia, N. Hou, Y. Zheng, and T. Gu, "Revolutionizing lora gateway with xgate: Scalable concurrent transmission across massive logical channels," in *ACM MobiCom*, 2024, pp. 482–496.
[42] J. P. S. Sundaram, W. Du, and Z. Zhao, "A survey on lora networking: Research problems, current solutions, and open issues," *IEEE Communications Surveys & Tutorials*, vol. 22, no. 1, pp. 371–388, 2019.
[43] C. Li and Z. Cao, "Lora networking techniques for large-scale and long-term iot: A down-to-top survey," *ACM Computing Surveys (CSUR)*, vol. 55, no. 3, pp. 1–36, 2022.
[44] Z. Sun, H. Yang, K. Liu, Z. Yin, Z. Li, and W. Xu, "Recent advances in lora: A comprehensive survey," *ACM Transactions on Sensor Networks*, vol. 18, no. 4, pp. 1–44, 2022.
[45] A. W. Azim, A. Bazzi, R. Shubair, and M. Chafii, "Chirp spread spectrum-based waveform design and detection mechanisms for lpwan-based iot–a survey," *IEEE Access*, 2024.
[46] Z. Wang, L. Kong, K. Xu, L. He, K. Wu, and G. Chen, "Online concurrent transmissions at lora gateway," in *IEEE INFOCOM 2020-IEEE Conference on Computer Communications*. IEEE, 2020, pp. 2331–2340.
[47] N. Hou, X. Xia, and Y. Zheng, "Don't miss weak packets: Boosting lora reception with antenna diversities," *ACM Transactions on Sensor Networks*, vol. 19, no. 2, pp. 1–25, 2023.
[48] X. Xia, Y. Zheng, and T. Gu, "Ftrack: Parallel decoding for lora transmissions," in *Proceedings of the 17th Conference on Embedded Networked Sensor Systems*, 2019, pp. 192–204.
[49] S. Tong, Z. Xu, and J. Wang, "Colora: Enabling multi-packet reception in lora," in *IEEE INFOCOM 2020-IEEE Conference on Computer Communications*. IEEE, 2020, pp. 2303–2311.
[50] S. Tong, J. Wang, and Y. Liu, "Combating packet collisions using non-stationary signal scaling in lpwans," in *Proceedings of the 18th International Conference on Mobile Systems, Applications, and Services*, 2020, pp. 234–246.
[51] Z. Xu, P. Xie, and J. Wang, "Pyramid: Real-time lora collision decoding with peak tracking," in *IEEE INFOCOM 2021-IEEE Conference on Computer Communications*. IEEE, 2021, pp. 1–9.
[52] X. Xia, N. Hou, Y. Zheng, and T. Gu, "Pcube: Scaling lora concurrent transmissions with reception diversities," *ACM Transactions on Sensor Networks*, vol. 18, no. 4, pp. 1–25, 2023.
[53] F. Yu, X. Zheng, L. Liu, and H. Ma, "Enabling concurrency for non-orthogonal lora channels," in *Proceedings of the 29th Annual International Conference on Mobile Computing and Networking*, 2023, pp. 1–15.
[54] A. Gamage, J. Liando, C. Gu, R. Tan, M. Li, and O. Seller, "Lmac: Efficient carrier-sense multiple access for lora," *ACM Transactions on Sensor Networks*, vol. 19, no. 2, pp. 1–27, 2023.
[55] Z. Xu, P. Xie, J. Wang, and Y. Liu, "Ostinato: Combating lora weak links in real deployments," in *2022 IEEE 30th International Conference on Network Protocols (ICNP)*. IEEE, 2022, pp. 1–11.
[56] P. J. Marcelis, V. Rao, and R. V. Prasad, "Dare: Data recovery through application layer coding for lorawan," in *Proceedings of the Second International Conference on Internet-of-Things Design and Implementation*, 2017, pp. 97–108.
[57] A. Dongare, R. Narayanan, A. Gadre, A. Luong, A. Balanuta, S. Kumar, B. Iannucci, and A. Rowe, "Charm: exploiting geographical diversity through coherent combining in low-power wide-area networks," in *2018 17th ACM/IEEE International Conference on Information Processing in Sensor Networks (IPSN)*. IEEE, 2018, pp. 60–71.
[58] A. Balanuta, N. Pereira, S. Kumar, and A. Rowe, "A cloud-optimized link layer for low-power wide-area networks," in *Proceedings of the 18th International Conference on Mobile Systems, Applications, and Services*, 2020, pp. 247–259.
[59] W. Mao, Z. Zhao, K. Zheng, and G. Min, "Recovering packet collisions below the noise floor in multi-gateway lora networks," in *IEEE INFOCOM 2023-IEEE Conference on Computer Communications*. IEEE, 2023, pp. 1–10.
[60] X. Xia, Q. Chen, N. Hou, Y. Zheng, and M. Li, "Xcopy: Boosting weak links for reliable lora communication," in *Proceedings of the 29th Annual International Conference on Mobile Computing and Networking*, 2023, pp. 1–15.
[61] LoRa Alliance, "Lorawan Specifcation," 2022. [Online]. Available: https://lora-alliance.org/about-lorawan
[62] Semtech, "SX1302," n.d., retrieved by Nov 13 2023. [Online]. Available: https://www.semtech.com/products/wireless-rf/loracore/sx1302
[63] Semtech, "SX1303," n.d., retrieved by Nov 13 2023. [Online]. Available: https://www.semtech.com/products/wireless-rf/loracore/sx1303
[64] Gr-LoRa GitHub community, "gr-lora projects," 2021. [Online]. Available: https://github.com/rpp0/gr-lora
[65] Semtech, "SX1278/77/78/79 Datasheet," n.d., retrieved by Nov 25 2023. [Online]. Available: https://www.semtech.com/products/wireless-rf/lora-core/sx1278